# Current Interruption by Density Depression

*J.S. Wagner* and T. Tajima*
Institute for Fusion Studies
The University of Texas at Austin
Austin, Texas 78712
and
*S.-I. Akasofu*
Geophysical Institute
University of Alaska
Fairbanks, Alaska 99701

## Abstract

Using a one-dimensional electrostatic particle code, we examine processes associated with current interruption in a collisionless plasma when a density depression is present along the current channel. Current interruption due to double layers was suggested by Alfvén and Carlqvist (1967) as a cause of solar flares. At a local density depression, plasma instabilities caused by an electron current flow are accentuated, leading to current disruption. Our simulation study encompasses a wide range of the parameters in such a way that under appropriate conditions, both the Alfvén and Carlqvist (1967) regime and the Smith and Priest (1972) regime take place. In the latter regime the density depression decays into a stationary structure ("ion-acoustic layer") which spawns a series of ion-acoustic "solitons" and ion phase space holes travelling upstream. A large inductance of the current circuit tends to enhance the plasma instabilities.

* *present address: Sandia Laboratory, Albuquerque, NM*

## I. Introduction

Alfvén and Carlqvist (1967) proposed that solar flares may be a consequence of localized current interruption along a magnetic flux tube, resulting in the explosive release of stored magnetic energy. In their model, when the current-carrying electron's drift speed $v_d$ exceeds a certain threshold value $v_c$, a density perturbation tends to grow. In particular, if a density depression is present or externally caused, it will grow. This is because the current carrying electrons must increase their drift speed ($v_d'$ in the depression) in order to preserve current continuity. The increase in the speed of the current carrying electrons as they pass through the depression sets up an additional voltage drop and increases the depth of depression. They expected that when the depression became deep enough, a double layer would be formed, becoming a source of a large resistance. Most of the magnetic energy in the current system would then be rapidly released in the double layer as energetic particles. These particles in turn should cause most of the solar flare phenomena observed.

However, Smith and Priest (1972) argued that the Alfvén-Carlqvist mechanism would not occur because the ion-acoustic instability has a lower threshold, $c_s \simeq (T_e/m_i)^{1/2}$. However, ion-acoustic instability occurs only when the electron temperature sufficiently exceeds the ion temperature. In fact, the Alfvén and Carlqvist model is supported by the experiments by Torvén (1979) and others.

In this paper we use a particle simulation method to study the initial value problem of an electron current flow through a local density depression. We primarily concentrate on cases where the electron temperature is higher than the ion temperature. Thus, the instabilities induced by the current in or near the density depression may include the electron (two-stream) instability (Buneman, 1958) and the ion (ion-acoustic) instability (cf. Ichimaru, 1973). Both may altogether be called the current-induced instabilities of which properties vary monotonically with the relative drift velocity and the wavenumber (Jackson, 1960; Fried and Gould, 1961). We focus on cases in which critical conditions for various instabilities are realized at the depression region, but not anywhere else.

Our simulation study shows that the current interruption process can take place in two possible regimes. As the electron drift speed relative to the ions $v_d'$ in the depression exceeds approximately the thermal speed $v_{th}$ (the first regime), the two-stream instability occurs. The current in the depression region locally exceeds the two-stream instability threshold and causes plasma wave growth. This increases effective resistivity through

trapping and scattering of electrons. The increased resistivity can in turn reduce the drift velocity and thus enhance the depression.

This first regime is associated with large amplitude electrostatic waves that trap both electrons and ions, and creates a large resistivity. Thus, both the current interruption and the deepening of the density depression take place together. Both electrons and ions are heated as they pass through the density depression. The electrons are accelerated through the depression and are decelerated downstream. Ions are accelerated upstream and form a large pulse which decays slowly upstream of the depression. The density depression deepens in space. The most pronounced depression takes place where the current first encounters the depressed region.

However, if the electron temperature $T_e$ is higher than the ion temperature $T_i$, an increased resistivity and thus eventual current interruption can result even when the electron streaming velocity $v_d'$ is less than the critical speed $u_c \approx v_{th} = (T_e/m_e)^{1/2}$, provided $v_d'$ is larger than the acoustic speed $c_s$. This is the second regime. (We may call this the ion-acoustic regime.) Here the ion-acoustic waves are not heavily damped if $T_e >> T_i$ (Fried and Gould, 1961.) This second regime is associated with ion-acoustic waves in the density depression that trap and heat the ions. The waves do not significantly affect the electrons. Hence the ions are heated but the electrons are not. The depression becomes deeper on the upstream edge of the depression, ejecting a pulse of ions from the depression in the upstream direction.

The ultimate fate of the ion-acoustic regime is the formation of a series of stationary ion-acoustic structures and the emission of them into the non-depressed (stable) region. Structures similar to these ion-acoustic structures in a uniform-current-carrying plasma of $c_s < v_d < v_{th}$ and $T_e \gg T_i$ were observed by Sato and Okuda (1980) who called them ion-acoustic double layers. DeGroot et al. (1977) observed similar features in computer simulation double layers in a uniform plasma when $v_d > v_{th}$ and $T_e \gg T_i$. However they are different from the conventional double layers (Block, 1972; Kan and Lee, 1979, Wagner et al., 1980). In such papers such structures are referred to as the acoustic layers. The acoustic layers appear quasi-periodically. Each acoustic layer is associated with a sharply growing density depression that increases until $\frac{\delta n}{n} \sim 0.5$. In ion phase space the growing density depression reflects the ions moving in the direction of the current- carrying electron flow. As the depression grows, ions are evacuated from the region and are ejected against the electron flow, forming a deepening depression in ion phase space. The depression in ion phase space turns into a hole in phase space as positive moving ions move in the direction of electron flow. Once the hole is filled, the process is repeated, whereby the depression deepens and decays, again forming a "soliton" and a hole in phase space. In the following, we present two cases, I and II, describing in detail the results of our simulation.

## II. Simulation Results

We investigate nonlinear aspects of the electrostatic interaction of a current-carrying plasma and a density depression. In order to carry out a self-consistent study of this nonlinear interaction, we use a standard one-dimensional electrostatic particle code (e.g. Birdsall, Langdon, and Okuda, 1970) with a periodic boundary condition. A cubic spline

interpolation technique first utilized to a particle simulation by Okuda and Cheng (1981) was used to reduce unnecessary noise due to particle fluctuations. Typical ranges for the parameters of the simulation are: the system length $L_x = 1024\Delta$, the electron thermal speed $v_{th} = 0.25\omega_p\Delta$ to $1\omega_p\Delta$ (thus the electron Debye length $\lambda_{De}$ range from $0.25\Delta$ to $1\Delta$), 40 electrons and ions per cell, the electron to ion temperature ratio $T_e/T_i = 3$ to 10, the ion to electron mass ratio $m_i/m_e = 64$, the simulation time step $\Delta t = 0.2\omega_d^{-1}$, where $\Delta$ is the unit grid spacing and $\omega_p$ is the electron plasma frequency outside of the plasma density depression at the initial time. The length of the density depression is taken as $L_{dep} = 64\lambda_{De}$.

In the following, we concentrate on the description of a canonical case. In this case we have the electron drift velocity outside of the depression $v_d$ less than the electron thermal velocity $v_{th}$ and the electron drift velocity in the depression $v_d'$ larger than $v_{th}$, where $v_{th} = (T_e/m_e)^{1/2}$. The following describes the nonlinear evolution of the canonical case.

*Case I* $\quad \frac{n_{dep}}{n} = 0.6, \quad v_d = 0.75v_{th}, \quad \frac{T_e}{T_i} = 5, \quad L_{dep} = 64\lambda_{De}.$

In this case the other parameters are the ones mentioned as typical at the beginning of this section (with $v_{th} = 1\omega_p\Delta$). Electrons drift from left to right. The temperatures are initially uniform in and outside of the depression. Outside the depression the electrons drift with speed $v_d = 0.75v_{th}$ and $v_{th} = 1\omega_p\Delta$. Because the electron current conserves in the depression the electrons drift with speed $v_d' = 1.25v_{th}$ which slightly exceeds the critical velocity $v_c \sim v_{th}$ in the depressed region. The condition for instability is approximately $v_d' > v_{th}$ and hence the instability is of oscillations of electron nature. It may be called the Buneman threshold. Figure 1 shows the initial density profile. Figure 2 shows time history of electron phase space and ion phase space for this canonical case. Overall, ions are initially at rest. In Fig. 2, results associated with the electrons are shown in the left column [Figs. 2(a-c)], while results associated with the ions are shown in the right column [Figs. 2(d-f)]. Figure 2(a) shows the initial electron phase space ($x$ vs. $v_x$), while Fig. 2(d) shows the initial ion phase space.

Figure 2(a) shows that electrons in the depressed region ($x \sim 512\Delta \pm 30\Delta$) travel faster, as a higher (positive) velocity in $x$-direction indicates. Figure 2(b) shows the electron phase space at a later time, $t = 240\omega_p^{-1}$. Large amplitude electrostatic waves have now been excited in the depressed region because of the electron ion two-stream instability above the threshold $v_d' > v_{th}$ at the depression. We can also see waves excited downstream

($x \leq 800\Delta$) as the striation-like structure indicates. A number of electrons are trapped and heated by the waves there. A net potential drop (not shown here) exists across the density depression so that electrons with negative velocities cannot cross the depression and are absent on the left (upstream) side of the depression. Electrons drifting in the positive direction are accelerated across the region. This is typical of the conventional double layer. A double layer-like structure is created by the density depression and the current. The electron energy is dissipated downstream in the turbulence generated by the electron-ion two-stream instability.

Figure 2(c) shows the electron phase space at a later time $t = 760\omega_d^{-1}$. The characteristic features of phase space mentioned above in this regime (i.e., $v_d' > v_{th}$) have decayed by this time $t = 760\omega_d^{-1}$, since the enhanced resistivity slowed down the electrons. The electron drift velocity $v_d'$ in the depression decreases until it became less than $v_{th}$ (i.e., $v_d' < v_{th}$); the system has entered the second regime in which the electron drift velocity $v_d'$ in the depression is less than the thermal velocity but still larger than the ion-acoustic speed $c_s \simeq (T_e/m_i)^{1/2}$. Thus we may call the former regime as the Buneman regime (i.e., $v_d' > v_{th}$) and the latter as the ion-acoustic regime (i.e., $c_s < v_d' < v_{th}$). Now at this stage electron phase space shows some modulation in the depression area but no trapping of electrons in the waves. The ion-acoustic waves are not large enough to trap and heat the electrons. This feature will later be contrasted with the simultaneous ion feature [Fig. 2(f)].

Figure 2(e) shows ion phase space at $t = 240\omega_p^{-1}$ corresponding to Fig. 2(b). The plasma waves driven by the electron-ion two-stream and net-potential drop across the depression are beginning to accelerate some of the ions in the negative (upstream) direction, and trap others in the waves. The ions are heated 2-5 times their initial thermal energies. From Figs. 2(d)-(e) we see ion phase space which shows that the averaged ion speed goes negative in the depression region. The majority of ions in the depressed region show a negative velocity with a maximum of the absolute value of the ion velocity $v_i = 0.23\omega_p\Delta$. This is greater than sound speed $c_s \simeq (T_e/m_i)^{1/2} \simeq 0.13\omega_p\Delta$. The ion phase space in Fig. 2(f) shows that the waves are trapping the ions. In addition, Fig. 2(f) shows that a potential drop is present across the developed depression region which prevents upstream ions with positive velocities from crossing the depression. Hence, Fig. 2(f) shows absence of ions with positive velocities on the downstream side of the depression. A large pulse moving left (negative velocities) in the region $375\Delta < x < 475\Delta$ seen in Fig. 2(f) are those

ions ejected from the depression during the Buneman phase of the instability. The density pulse is still travelling upstream with slightly supersonic Mach number of $M = 1.1$.

Figures 3(a) and (b) exhibit a series of ion-distribution functions (space averaged) at two stages. Figures 3(c) and (d) show the corresponding ion density profiles. The ions deepen the depression more significantly on the upstream edge, $\left(\frac{n_{dep}}{n}\right)_{t=240\omega_d^{-1}} = 0.45$, compared to an initial value of $\left(\frac{n_{dep}}{n}\right)_{t=0} = 0.6$. This tendency of creating the upstream structure is due to the backstreaming ions as seen in Fig. 2. The pulse can also be seen in the plot of ion density Fig. 3(d). The pulse has an amplitude of $\frac{\delta n}{n} \sim 0.2$, while the density depression has relaxed to a depth of $\frac{n_{dep}}{n} \sim 0.6$ (very close to its initial value).

The time history of various values of plasma parameters is given in Fig. 4. Figure 4(a) shows the electron temperature $T_e$ (space averaged) as a function of time. During the phase when the Buneman instability is active, the electrons are heated to 1.3 times their initial temperature. After the current is interrupted to the point where plasma waves are no longer unstable in the depression, at about time $\sim 500\omega_d^{-1}$, the electron temperature no longer increases, but saturates and slowly decreases. Figure 4(b) shows the ion temperature (space averaged) as a function of time. The ions are heated from $T_i = 0.2T_e(t = 0)$ at $t = 0$, to a final value of $T_i = 0.28T_e(t = 0)$, and continue to increase in temperature during the ion-acoustic regime. Figure 4(c) shows the electron current as a function of time. The mean velocity of the electrons is reduced from an initial value of $0.75v_{th}$ to a final value of $0.42v_{th}$, a reduction of 44% within a matter of $600\omega_d^{-1}$ time.

In this canonical case for the Alfvén and Carlqvist regime, the density depression grows in time (maximum depression at $n_{dep}/n \sim 0.45$), causing the strong electron-ion two-stream instability and ensuing plasma turbulence. The current has decreased by almost 50% over this period ($\sim 600\omega_{pe}^{-1}$ time). After this phase the system evolves only very slowly, as the two-stream (Buneman) instability has been saturated by current interruption itself and the resulting heating. There appears an upstream travelling pulse structure.

*Case II* $\quad \frac{n_{dep}}{n} = 0.85, \quad v_d = 0.75v_{th}, \quad \frac{T_e}{T_i} = 5, \quad L_D = 64\lambda_{De}.$

This case is the same as the previous case, except that the density depression is now $\frac{n_{dep}}{n} = 0.85$, instead of $\frac{n_{dep}}{n} = 0.6$ as in Case I: The maximum drift velocity of the electrons in the depression is now $0.88v_{th}$, less than the Buneman threshold for the two-stream instability. Notice that the temperature ratio $T_e/T_i = 5$ causes the ion-acoustic instability under appropriate conditions. This case represents a typical case for the second

(ion-acoustic) regime *ab initio*. The ion-acoustic waves are excited in the depression and ion-acoustic turbulence develops, since the ion-acoustic instability condition ($c_s < v_d' < v_{th}$) is satisfied there in this case. On the other hand, if $T_e$ is not much larger than $T_i$ (Fried and Gould, 1961), this second regime does not exist, since the ion-acoustic wave does not become unstable in such a case. The waves trap and heat ions, but do not trap electrons. The depression develops and deepens, as was the case in the first regime.

Figure 5 displays various stages of electron and ion phase space. Figure 5(a) shows the electron phase space at $t = 750\omega_d^{-1}$, while Fig. 5(d) shows the ion-phase space at the same time. In this case electron phase space is perturbed only a little, while ion phase space shows a significant backstreaming and trapping, and eventually a hole structure near $x = 600\Delta$ in phase space [Fig. 5(f)], in contrast with the case in Fig. 2.

Figure 6 shows the development of ion density profile. Figure 6(a) shows the ion density at $t = 750\omega_d^{-1}$. One can see that the initial ion-acoustic turbulence has given rise to a single ion-acoustic structure. A similar structure was observed by Sato et al., (1980). The main features in Figs. 5 and 6 are illustrated schematically in Fig. 7, and it may be instructive to refer to Fig. 7 when Fig. 6 is examined in detail. Detailed inspection of a large number of phase space plots similar to those shown in Fig. 5 indicates that this layer is decaying, emitting a solitary pulse of ions travelling approximately at the ion-acoustic speed $c_s$ against the electron drift (upstream propagation). A decaying hole in ion phase space is also observed. At $t = 1250\omega_d^{-1}$ another ion-acoustic layer begins to form at the downstream edge of the initial perturbation (depression) and is shown in Figs. 5(b), 5(e), 6(b). At a later time $t = 1750\omega_d^{-1}$ the layer structure has decayed, leaving a hole in ion phase space. No remarkable disturbance is observed in the electron phase space. This process repeats itself as indicated schematically in Fig. 7 [after phase (viii) is reached, the cycle comes back to phase (iii)].

Figure 8(a) shows the space-averaged electron-temperature history $T_e(t)$, while Fig. 8(b) shows the ion temperature history $T_i(t)$ over the length of the run. Figure 8(c) shows the electron current history. The electron current history in Fig. 8(c) shows several features discussed earlier which occur during the current decrease. The initial decrease, up to $450\omega_d^{-1}$, occurs while the current drives the ion-acoustic turbulence. From $450\omega_d^{-1}$ to $900\omega_p^{-1}$ an ion-acoustic layer forms and decays at the upstream-edge of the density depression. The arrow at $t = 900\omega_d^{-1}$ indicates the time for the layer decay. The current levels off from $900\omega_d^{-1}$ to $1000\omega_d^{-1}$. After $1000\omega_d^{-1}$ another layer forms on the downstream-

edge of the depression, current decays at a slow rate until the second ion-acoustic layer decays at $1900\omega_d^{-1}$. The second arrow at $t = 1900\omega_d^{-1}$ marks this time. At each of the layer decay time, the electron current decreases less rapidly [Fig. 8(c)]. At this point the current density has dropped from $0.75nev_{th}$ to $0.5nev_{th}$, a drop of 30% of the current. The electron-temperature history shows a slower heating than at earlier times. Its heating rate goes down after the decay of the first hole. The net increase in electron temperature through the duration of the run is +22%. The ions are heated linearly in time until the second ion-acoustic layer decays. The final ion temperature shows a net gain of 32% at the end of this run.

In this case with a small initial density depression, which satisfies the condition $c_s < v_d' < v_{th}$ at the depression, the density depression can still grow in time. This is accompanied by the ion-acoustic instability and its turbulence. A density hill (pulse) appears upstream of the depression. This pulse structure propagates upstream with a speed slightly higher than at the speed of sound. The current decrease is again substantial (more than 50%) over the length of the run ($2000\omega_d^{-1}$).

## III. Summary and Discussion

We have studied the current interruption process in several parameter regimes and our results are summarized in Table I. All the qualitative physical results fall into the previous two cases.

In these runs we started from a given current value and let the system evolve. The system is insulated from the external circuitry, because there exists no external parameter such as the external field. In their model of solar flares, Alfvén and Carlqvist considered that the inductance of the current loop is large and thus the current decrease should be quickly compensated for by the loop-current circuit. Considering this situation, we also run a case in which the current in the simulation system is monitored in such a way that the initial current value is quickly recovered. For this purpose, we applied an electric field that is uniform in space ($E_{dc}$) to overcome the current decay at each time step. The condition we adopted was that $E_{dc} = \alpha(J_0 - J)$ with the initial current density, $J_0$ and $J$ is the current at a given time, $\alpha$ is a constant, and $E_{dc}$ is a *dc* electric field applied at the next time step of the given time. The *dc* field is applied in such a way that any current excess (or lack of it) is compensated for by the field in the next time step. This condition may be rewritten as $L\Delta J/\Delta t = E_{dc}\ell$ with $\ell$ being the length of the plasma. A

large value of $\alpha$ could correspond to a large inductance and thus corresponds to a quick recovery of the current to the original value. Simulation under this condition has been carried out, in which the initial current stays approximately constant at $J_e = 0.76nev_{th}$ [see Fig. 9(g)]. The simulation yields otherwise essentially the same qualitative results on the density depression dynamics and wave evolution. Typical results are shown in Fig. 9. The density depression at $t = 1000\omega_d^{-1}$ is $n_{dep}/n \sim 0.6$ for the equivalent parameters of Case I. The current, however, rapidly oscillates around the initial value, seen in Fig. 9(g). One can infer then that when the external circuit is applied, it can act to prolong the regime of the density depression.

In conclusion, current decrease at localized density depressions can occur in two regimes: a two-stream instability regime characterized by rapid current decay, and electron (and ion) heating if the electron temperature is substantially higher than the ion temperature to allow for the ion-acoustic instability to grow; the ion-acoustic regime is characterized by a slower current interruption, electron heating, and ion heating. In this ion-acoustic regime, a series of ion-acoustic layers is generated: each layer resembles that observed by Sato and Okuda (1980) and analyzed by Hasegawa and Sato (1982). Current interruption is accompanied by deepening density depression and upstream travelling ion-acoustic pulses. The Alfvén-Carlqvist case corresponds to the former case, while the Smith-Priest case may be said to be a part of the latter case. Thus, our study encompasses the entire current interruption processes under the postulated circumstances by Alfvén and Carlqvist. The results obtained by Alfvén-Carlqvist (1967) and Smith and Priest (1972) are applicable under appropriate but limited conditions.

We found a recursive physical phenomenon in the ion-acoustic regime. Near or in the density depression the formation and the subsequent propagation of the density pulse against the electron stream with speed approximately $c_s$ was observed. This is accompanied by creation of an ion-phase space hole, which eventually dissolve. This process repeats. Such a remarkably sustained generation of clumps and holes is provided by the presence of the depression. The presence of phase-space clumps and holes (Berk and Roberts, 1970) is believed to enhance the resistivity and should contribute to current interruption (Dupree, 1972, 1982, 1983; Berman et al., 1983). From our investigations, it can be concluded that the density depression in the current channel triggers current interruption and it also causes various rich physical phenomena as described in the above.

It is worth noting that in the magnetosphere an interesting electric potential structure is found to form in the region of upward field-aligned currents, accelerating the current-carrying electrons to produce the aurora. It has also been found that the plasma density decreases considerably within the potential structure (Calvert, 1981), being $\sim 1/cc$ compared with $\sim 30/cc$ in the surrounding region. Kan et al., (1983) suggested that such a potential structure may also form in the upward field-aligned current region of the solar atmosphere. If this would indeed be the case, a density depression may occur in the potential structure, leading to current interruption as suggested by Alfvén and Carlqvist. Several authors, including Zakharov (1972), Kim, Stenzel, and Wong (1974) [also Leung et al., (1980)], and Goldman and Nicholson (1977) have also suggested mechanisms by which the (field-aligned) current leads to the creation of density depression.

**Acknowledgments**

We would like to thank Professors P. Carlqvist and H. Alfvén for helpful and enlightening discussions.

This work was supported by the National Science Foundation grants NSF ATM82-14730 to The University of Texas at Austin and the U.S. Department of Energy contracts DE-FG05-53088 and DE-AT06-76ER-7005 to The University of Texas at Austin and to the University of Alaska at Fairbanks, respectively.

## References


H. Alfvén and P. Carlqvist, Solar Phys. **1**, 220 (1967).

H.L. Berk and K.V. Roberts, Phys. Fluids **11**, 980 (1970).

R.H. Berman, D.J. Tetreault, and T.H. Dupree, Phys. Fluids **26**, 2437 (1983).

C.K. Birdsall, A.B. Langdon, and H. Okuda, in *Methods of Computational Physics* (Academic Press, New York, 1970) vol. 9, p. 241.

L.P. Block, Cosmic Electrodyn. **3**, 349 (1972).

O. Buneman, Phys. Rev. Lett. **1** 8 (1958).

W. Calvert, Geophys. Res. Lett. **8**, 919 (1981).

P. Carlqvist, Cosmic Electrodyn. **3**, 377 (1972).

P. Carlqvist, in *Wave Instabilities in Space Plasmas*, ed. by P.J. Palmadesso and K. Papadopoulos (Reidel, Holland, 1979), p. 83.

J.S. DeGroot, C. Barnes, A.E. Walstead, and O. Buneman, Phys. Rev. Lett. **38**, 1283 (1977).

T.H. Dupree, Phys. Fluids **15**, 334 (1972).

T.H. Dupree, Phys. Fluids **25**, 277 (1982) and Phys. Fluids **26**, 2460 (1983).

B.D. Fried and R.W. Gould, Phys. Fluids **4**, 139 (1961).

M.V. Goldman and D.R. Nicholson, Phys. Fluids **20**, 756 (1977).

A. Hasegawa and T. Sato, Phys. Fluids **25**, 632 (1982).

S. Ichimaru, *Basic Principles of Plasma Physics* (Benjamin, Reading, Massachusetts, 1973).

E.A. Jackson, Phys. Fluids **3**, 786 (1960).

E.A. Jackson, Phys. Fluids **5**, 786 (1960).

J.R. Kan, S.-I. Akasofu, and L. Lee, Solar Phys. **84**, 153 (1983).

J.R. Kan and L.C. Lee, J. Geophys. Res. **85**, 788 (1980).

H.C. Kim, R.L. Stenzel, and A.Y. Wong, Phys. Rev. Lett. **33**, 886 (1974).

P. Leung, A.Y. Wong, and B.H. Quong, Phys. Fluids **23**, 992 (1980).

H. Okuda and C.Z. Cheng, Comp. Phys. Comm. **14**, 169 (1978)

T. Sato and H. Okuda, Phys. Rev. Lett. **44**, 740 (1980).

D.F. Smith and E.R. Priest, Ap. J. **176**, 487 (1972).

S. Torven, in *Wave Instabilities in Space Plasmas*, ed. by P.J. Palmadesso and K. Papadopoulos (Reidel, Holland, 1979) p. 109.

J.S. Wagner, T. Tajima, J.R. Kan, J.N. Leboeuf, S.-I. Akasofu, and J.M. Dawson, Phys. Rev. Lett. **45**, 803 (1980).

V.E. Zakharov, Zh. Eksp. Teor. Fiz. **62**, 1745 (1972) [Sov. Phys. JETP **35**, 908 (1972)].

## Figure Captions

Fig. 1 Initial ion density profile. The average density out of the depression is normalized to unity.

Fig. 2 Phase space evolution in the first canonical case (initially the two-stream regime): $n_{dep} = 0.6$, $v_d = 0.75 v_{th}$, $T_e/T_i = 5$, $L_{dep} = 64\lambda_{De}$. (a)-(c) for electrons and (d)-(f) for ions. (a),(d) at $t = 0$; (b),(e) at $t = 240\omega_p^{-1}$; (c),(f) at $t = 760\omega_p^{-1}$. NB: Horizontal stripes that appear in some phase space plots are due to artifacts of the computer printout defects. Normalizations of figures are as follows: the velocity to $\omega_p\Delta$, the length to $\Delta$, time to $\omega_d^{-1}$, the current to $nev_{th}$, and the temperature to $T_e(0)$.

Fig. 3 Evolution of ion velocity distribution [(a) and (b)] and ion density [(c) and (d)]. (a) and (c) at $t = 240\omega_p^{-1}$; (b) and (d) at $t = 760\omega_p^{-1}$.

Fig. 4 Time history of electron (a) and ion (b) temperatures and current (c) in the first canonical case (Case I).

Fig. 5 Phase space evolution in the second canonical case (the ion-acoustic regime): $n_{dep}/n = 0.85$, $v_d = 0.75 v_{th}$, $T_e/T_i = 5$, $L_{dep} = 64\lambda_{De}$. (a)-(c) for electrons and (d)-(f) for ions. (a),(d) at $t = 750\omega_p^{-1}$ (b),(e) at $t = 1250\omega_p^{-1}$; (c),(f) at $t = 1750\omega_p^{-1}$.

Fig. 6 Evolution of ion density profile. (a) at $t = 750\omega_p^{-1}$; (b) at $t = 1250\omega_p^{-1}$; (c) at $5 = 1750\omega_p^{-1}$.

Fig. 7 Schematic evolution of the plasma density profile and ion phase space for the second case (the ion-acoustic regime). Early time (i) to later time (vii). Repetitions from (iii) to (vii) after one full circle.

Fig. 8 Time history of electron (a) and ion (b) temperatures and current (c) in the second canonical case (Case II).

Fig. 9 With the current maintained at approximately the initial value by the external dc electric field. The initial density depression is again around $x = 512\Delta$. (a) electron phase space at $t = 750\omega_p^{-1}$; (b) ion phase space at $t = 750\omega_p^{-1}$; (c) ion density profile at $t = 750\omega_p^{-1}$; (d) electron velocity distribution at $t = 750\omega_p^{-1}$; (e) electron temperature history; (f) ion temperature history;

(g) current as a function of time.

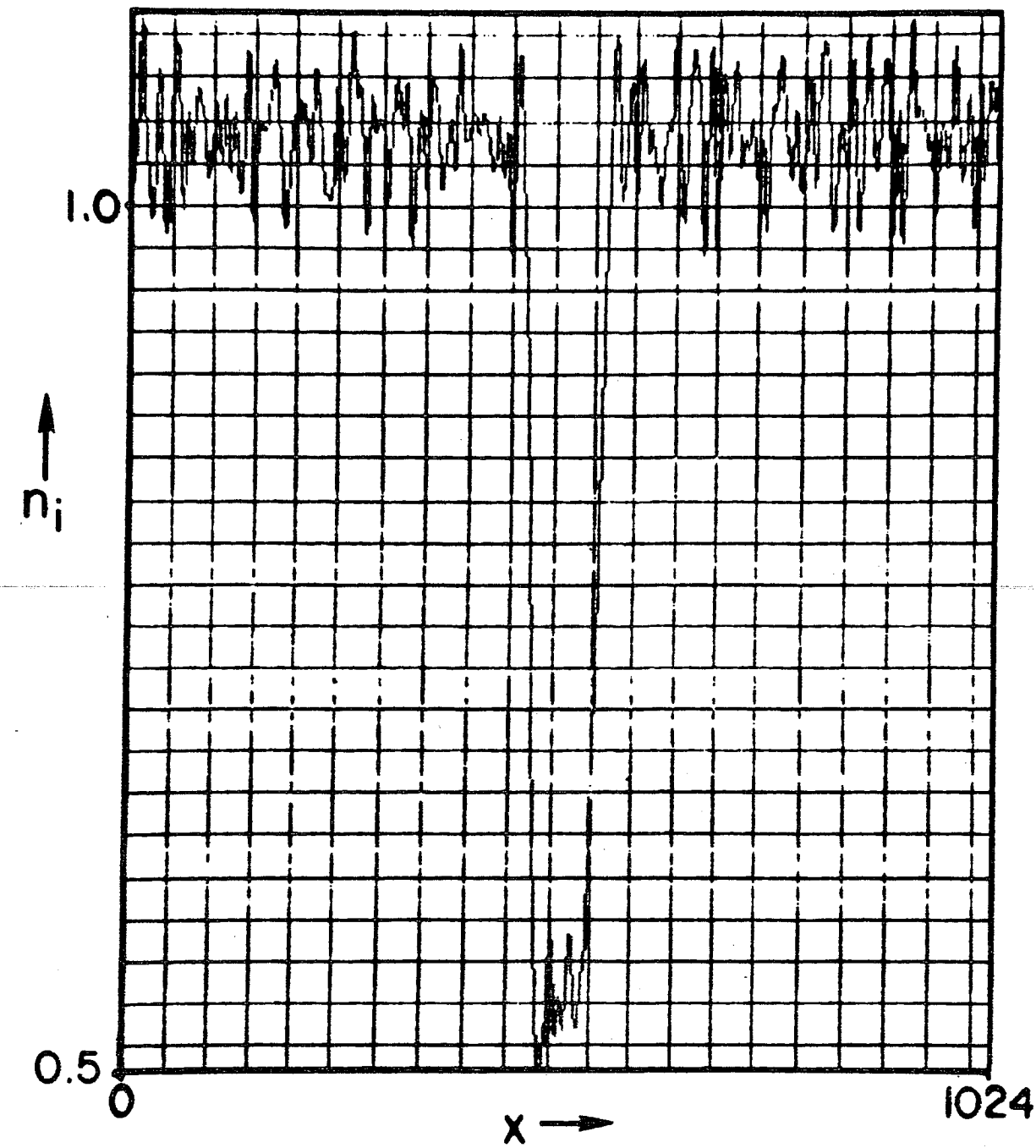


Fig. 1

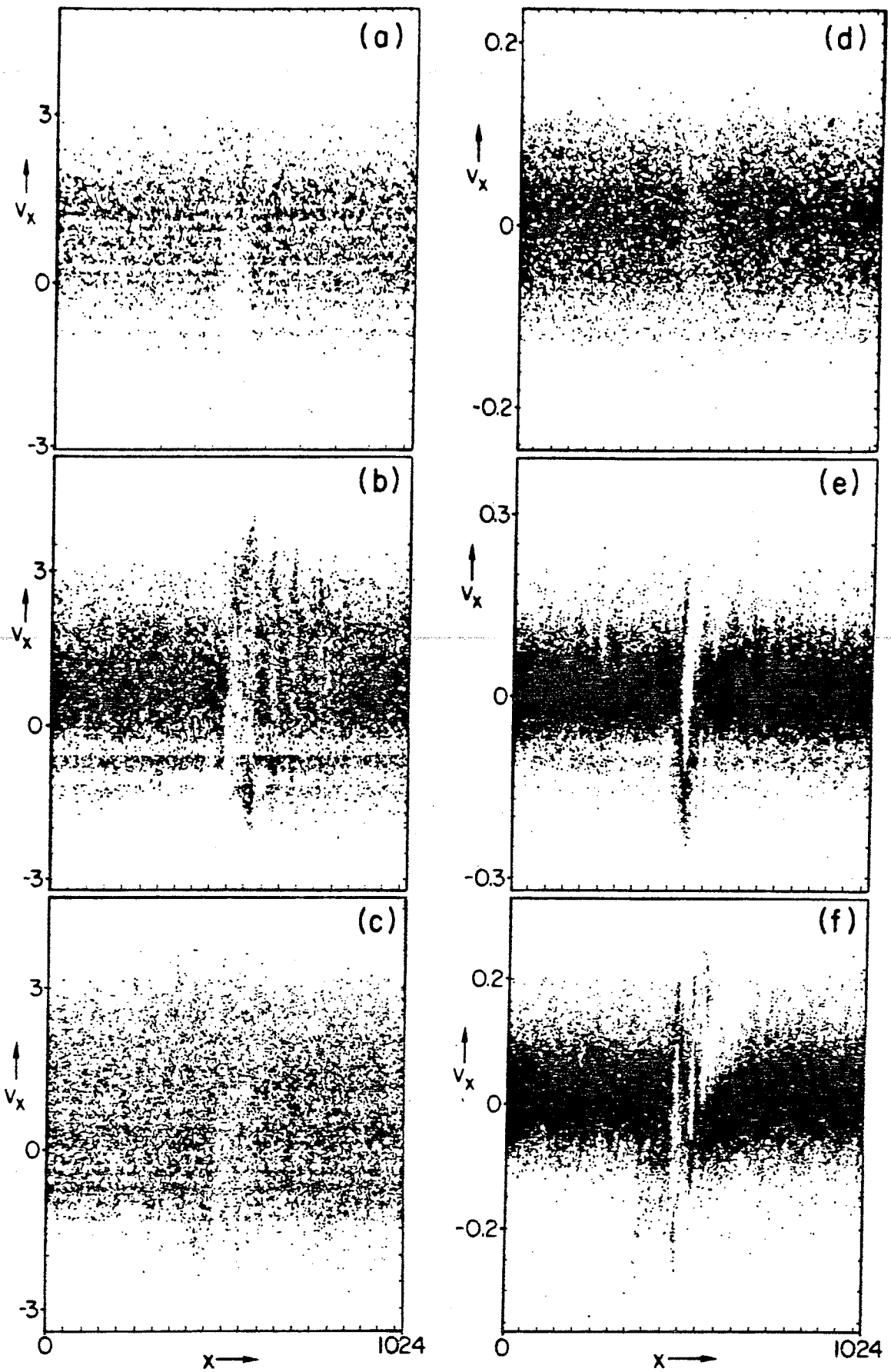


Fig. 2

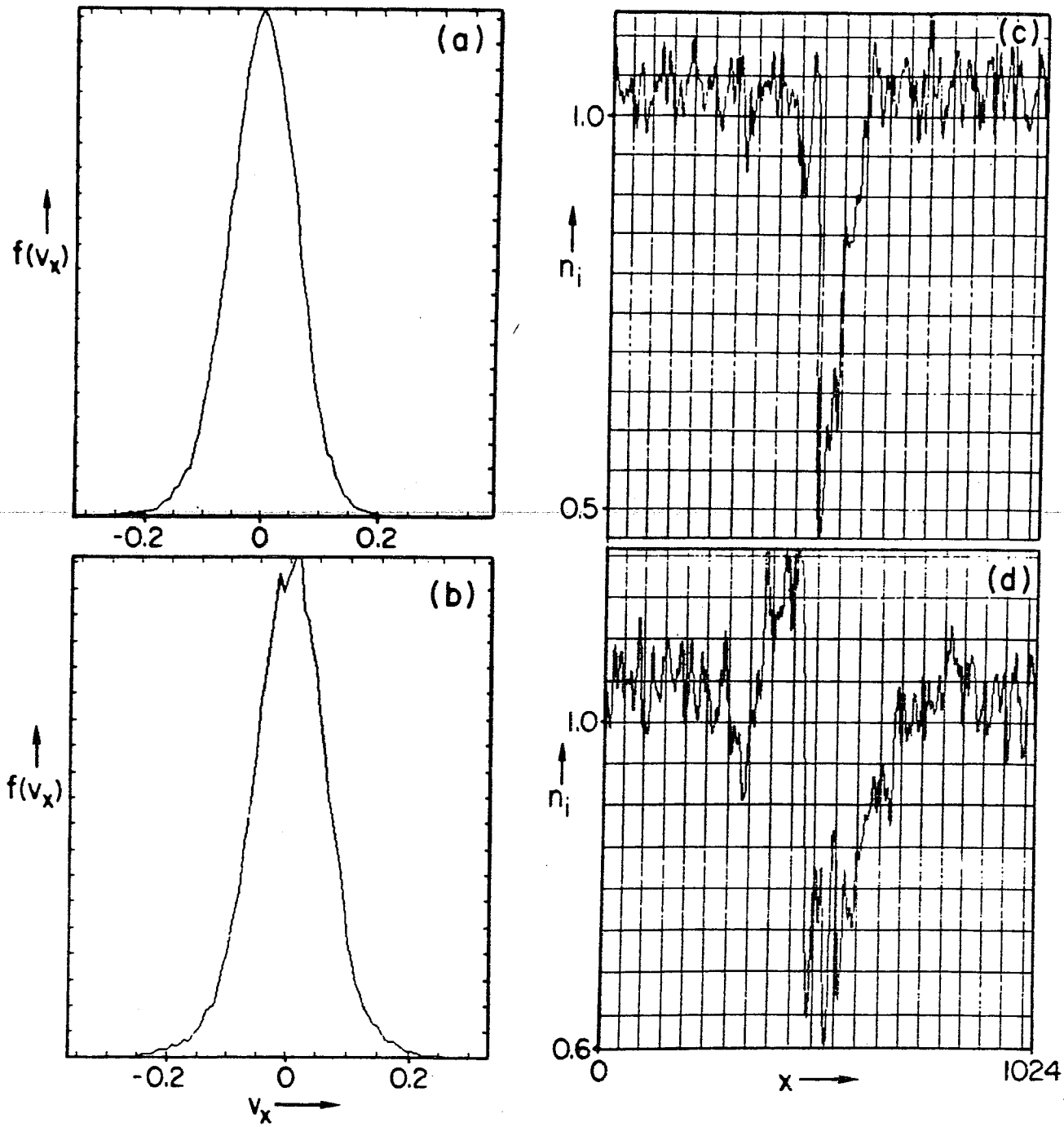


Fig. 3

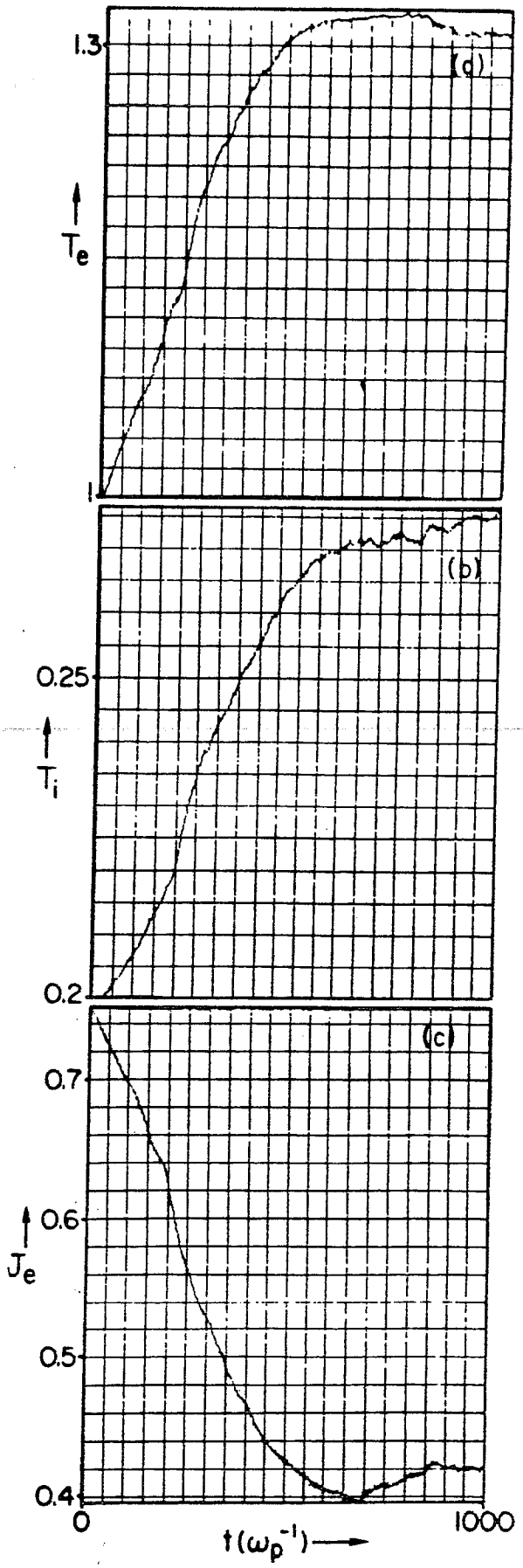


Fig. 4

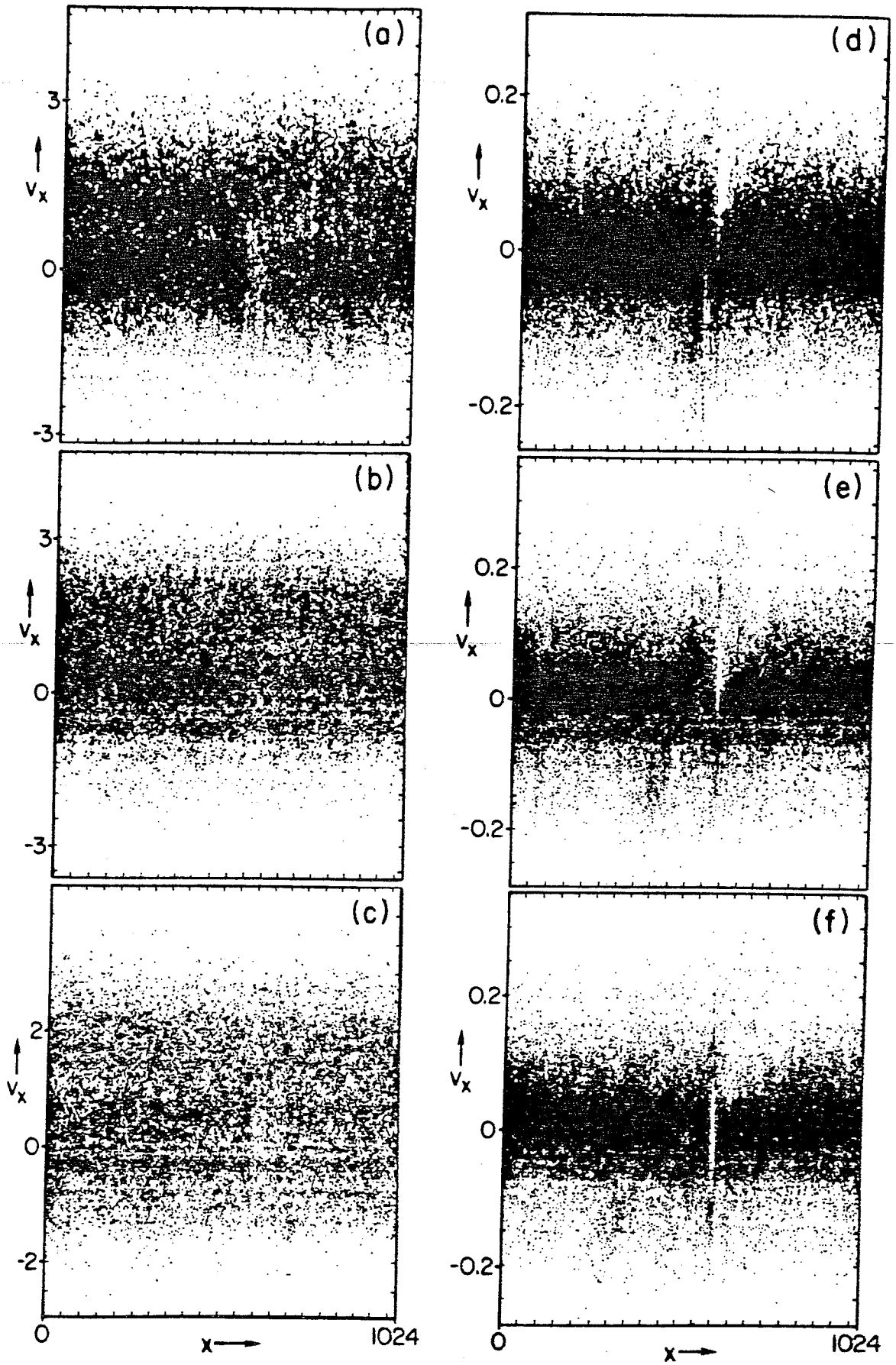
(a)
3
$v_x$
0
-3
(b)
3
$v_x$
0
-3
(c)
2
$v_x$
0
-2
0
x
1024
(d)
0.2
$v_x$
0
-0.2
(e)
0.2
$v_x$
0
-0.2
(f)
0.2
$v_x$
0
-0.2
0
x
1024

Fig. 5

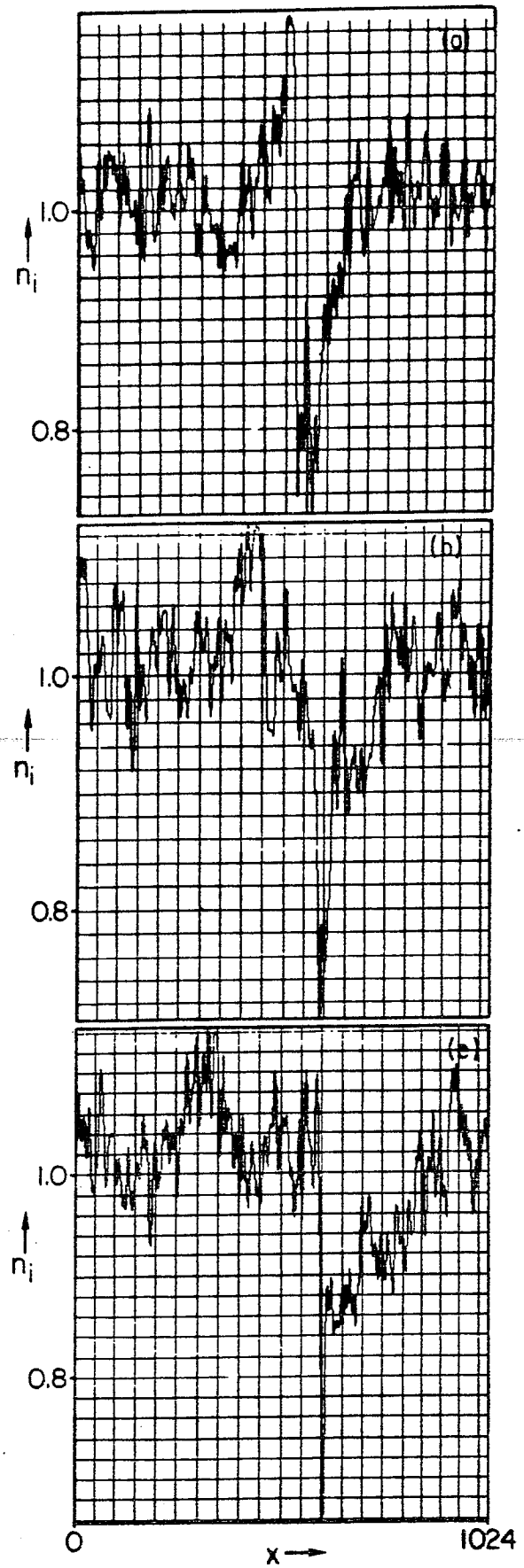


Fig. 6

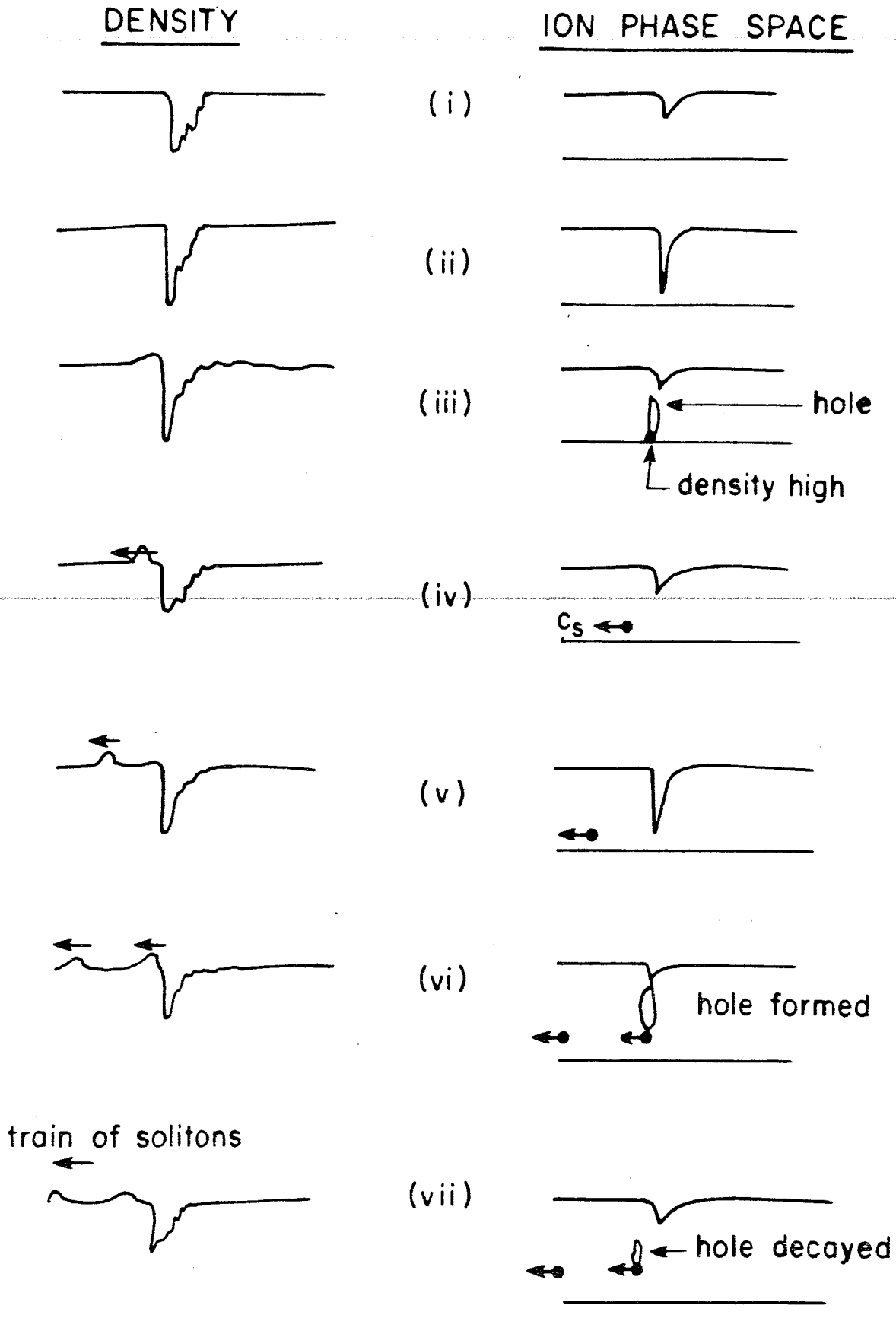
DENSITY
ION PHASE SPACE
(i)
(ii)
(iii)
hole
density high
(iv)
$C_S$
(v)
(vi)
hole formed
train of solitons
(vii)
hole decayed

Fig. 7

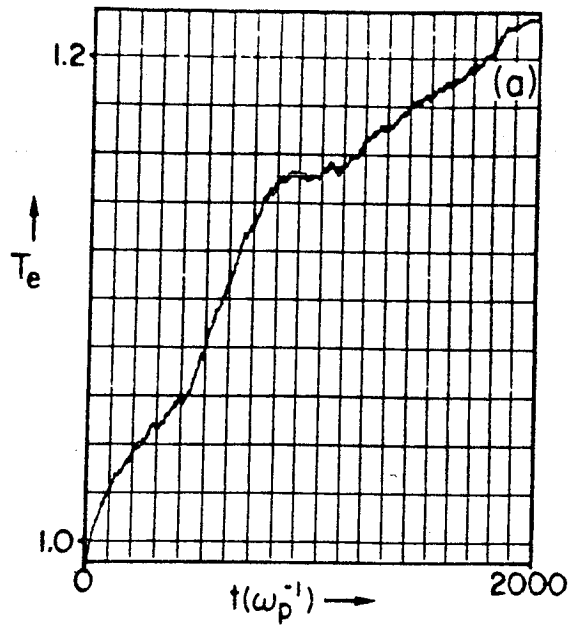
1.2
(a)
$T_e$
1.0
0
2000
$t(\omega_p^{-1})$

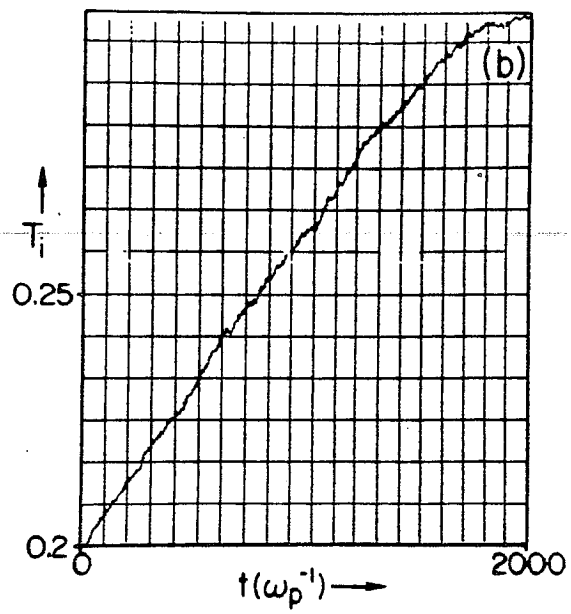
(b)
$T_i$
0.25
0.2
0
2000
$t(\omega_p^{-1})$

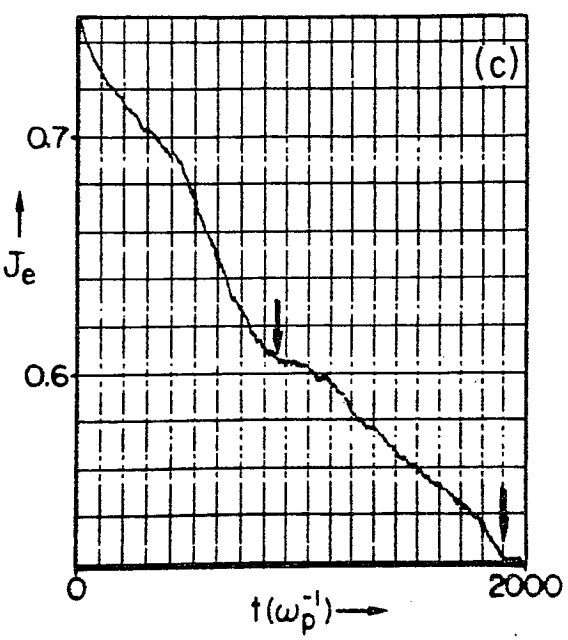
(c)
0.7
$J_e$
0.6
0
2000
$t(\omega_p^{-1})$

Fig. 8

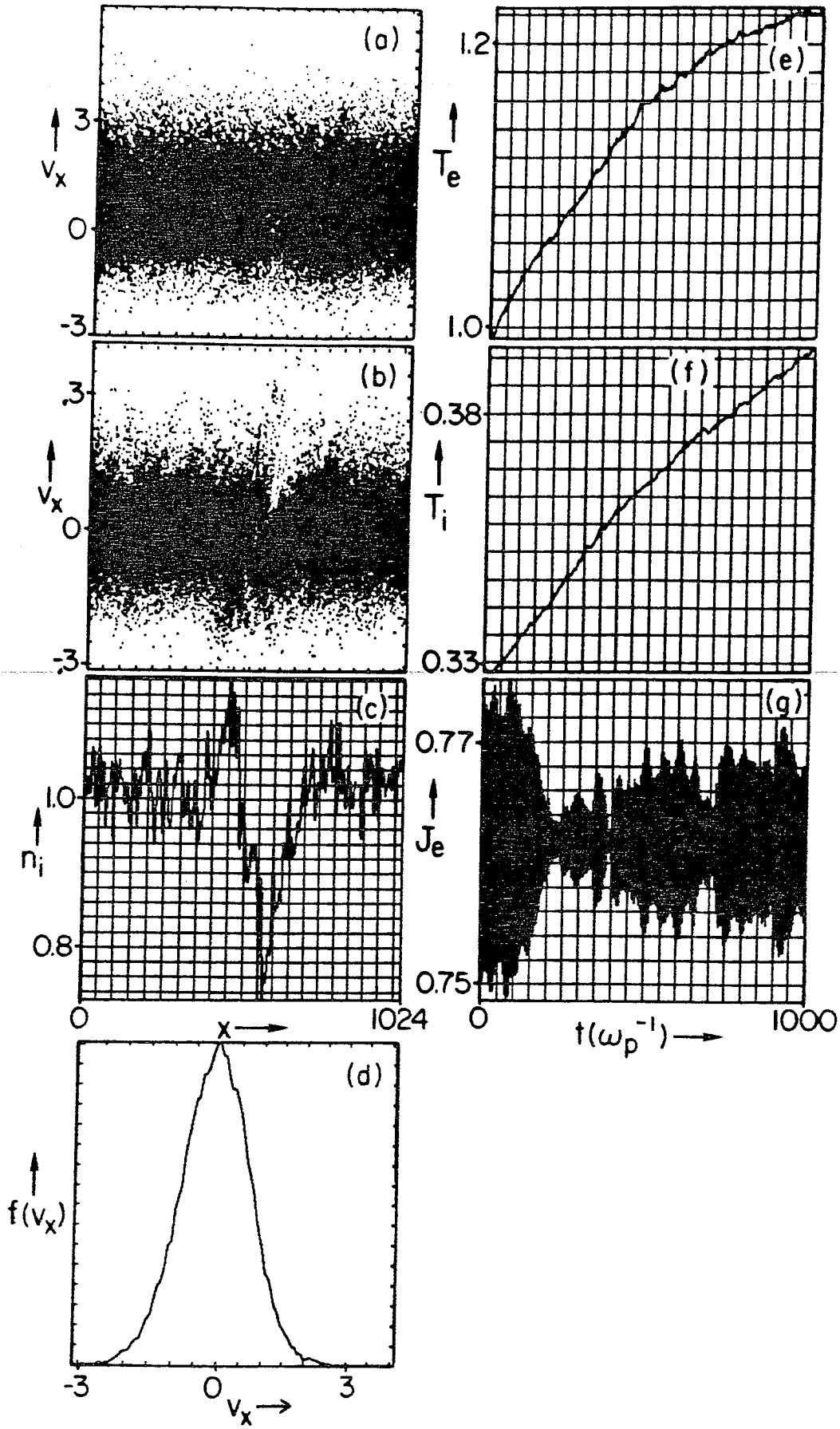
(a)
3
$V_x$
0
-3
(b)
3
$V_x$
0
-3
(c)
1.0
$n_i$
0.8
0
1024
x
(d)
$f(V_x)$
-3
0
3
$V_x$
(e)
1.2
$T_e$
1.0
(f)
0.38
$T_i$
0.33
(g)
0.77
$J_e$
0.75
0
1000
$t(\omega_p^{-1})$

Fig. 9